Thermopower in highly reduced *n*-type ferroelectric and related perovskite oxides and the role of heterogeneous nonstoichiometry

Soonil Lee,[1,*] Gaiying Yang,[1] Rudeger H. T. Wilke,[1,2] Susan Trolier-McKinstry,[1,2] and Clive A. Randall[1]
[1]*Center for Dielectric Studies, Materials Research Institute, The Pennsylvania State University, University Park, Pennsylvania 16802, USA*
[2]*W. M. Keck Smart Materials Integration Laboratory, Materials Research Institute, The Pennsylvania State University, University Park, Pennsylvania 16802, USA*
(Received 28 January 2009; published 16 April 2009)

Nonstoichiometric perovskite-structured alkaline-earth titanates with ferroelectric, paraelectric, and paraelastic phases were investigated for thermoelectric properties. Depending on the degree of reduction, different trends are noted. In ferroelectric $BaTiO_3$, thermopower anomalies are observed in and around the paraelectric (*Pm*3*m*)-ferroelectric (*P*4*mm*) and ferroelectric (*P*4*mm*)-ferroelectric (*Cmm*2) phase transition temperatures, and the nature of these trends was found to depend on the degree of reduction. This indicates a coupling between the thermoelectric effect and the ferroelectric phase transition, a phenomena also noted in the recent work of Kolodiazhnyi [T. Kolodiazhnyi, Phys. Rev. B **78**, 045107 (2008)]. Heavily reduced $SrTiO_{3-\delta}$ showed a strong metallic behavior in the thermopower and conductivity data without anomalies as the phase is paraelastic in the temperature range studied. The nature of the reduction from the low oxygen partial pressure anneals is heterogeneous; clusters of defects ~3 nm wide meander through the crystallites. The defective regions have high oxygen vacancy concentrations, and the chemical nature of the Ti changes from Ti^{4+} to Ti^{3+}. The complex nature of the thermochemical reduction near the metal-insulator transition will challenge simple physical models for oxide thermoelectrics. Traditional thermopower models are discussed in relation to the reported thermopower and the conductivity in the paraelectric and ferroelectric phases.

DOI: 10.1103/PhysRevB.79.134110 PACS number(s): 61.72.J−, 72.20.Pa, 71.30.+h

I. INTRODUCTION

There is an interest in finding new highly efficient thermoelectric materials for active cooling, energy harvesting, and thermal imaging devices. A simple first assessment of thermoelectric materials is through the figure of merit, *Z*, which involves the thermal conductivity, κ, electrical conductivity, σ, and Seebeck coefficient, $S=\Delta V/\Delta T$,[1] such that $ZT=S^2\sigma T/\kappa$.[2] For room-temperature applications, the highest reported *ZT* values for bulk materials are near 1 in semiconductor alloys based on Bi_2Te_3.[3] Most semiconducting alloys become unstable or exhibit lower *ZT* values at high temperatures, necessitating a search for novel materials that can more efficiently harvest waste energy at high temperatures. Based on the idea proposed by Slack[4] of a "phonon-glass electron crystal," the search has largely focused on crystal structures that can incorporate loosely bound "rattling" ions that in turn minimize thermal conductivity without significantly affecting the electrical transport properties (for a comprehensive review of many of the current issues in thermoelectric research see, e.g., Refs. 3, 5, and 6, and references therein). With the recent discovery of high thermopower in $NaCo_2O_4$,[7] there has been renewed interest in complex oxides, including those with the perovskite structure[8] for thermoelectric applications. The attractions of these materials include the low cost of the raw materials, the nontoxic elements, the possibility of high-temperature applications, the possibility of small, lightweight devices, and the potential low cost manufacturing with multilayer thick film technologies.

The reports by Yu *et al.*[9] and Ohta[6] indicated that high thermopower coefficients appear at the interfaces between $SrTiO_3$ and La-doped $SrTiO_3$ epitaxial thin films and heterostructures and $SrTiO_3/SrTi_{0.8}Nb_{0.2}O_3$ superlattices. Yu *et al.*[9] and Hicks and Dresselhaus[10] suggested that local reduction and low dimensionality are key parameters for the enhanced *n*-type thermopower or Seebeck coefficients, noting magnitudes of $600<|S|<1000$ μV/K with a negative sign consistent with a *n*-type carrier. Similarly, Frederikse *et al.*[11] reported high Seebeck coefficients in reduced bulk samples of $SrTiO_3$, $S\sim-750$ μV/K for $n_c\sim1\times10^{18}/cm^3$, while Kolodiazhnyi *et al.*[12] reported high Seebeck coefficients in reduced *Y*-doped $BaTiO_3$, $S\sim-550$ μV/K for $n_c\sim5\times10^{19}/cm^3$.

It is noteworthy that, in general, thermoelectric materials have high electronic carrier concentrations from $\sim10^{18}$ to 10^{21} carriers/cm^3. In many of the perovskite materials, these high carrier concentrations are very close to the insulator-metal transition, which can be estimated from the Mott criterion, $n_e^{1/3}a_0\sim0.25$, where n_e is the electronic carrier concentration and a_0 is the Bohr radius associated with the carrier and the dopant. a_0 depends on material properties such as the carrier effective mass and the dielectric permittivity.[13] When the Mott criterion exceeds 0.25, the conduction is metallic; below this point, the conduction is semiconducting or insulating. The transition between the two states is sometimes referred to as a metal-insulator transition, and has been extensively investigated in a wide variety of materials. In materials with high carrier concentrations, frequently there is departure from the nearly-free-electron model, and complex processes such as adiabatic small polaron and localized Anderson-variable hopping can control the electrical conductivity in perovskites.[14]

In this article, we demonstrate some examples of high thermopower coefficients in perovskite-related bulk materi-

TABLE I. Synthesis conditions and physical parameters for reduced alkaline-earth perovskite oxides; Δh_{Re} is the formation enthalpy for doubly ionized oxygen vacancy, n_e is the electron concentration estimated from the annealing conditions, n_e^1 and n_e^2 are the electron concentrations evaluated from m^*/m_e values (at $A=3$ and 4, respectively), which is estimated from the Seebeck coefficients (S) based on the relationship between m^*/m_e and S from Ref. 16, and HT and LT present high-temperature and low-temperature regions, respectively.

	Preparation			Carrier concentration		
Sample	Sintering	Annealing	Δh_{Re} (eV)	$n_e(n_e^1, n_e^2)$ ($\times 10^{19}$ cm^{-3})	Method	m^*/m_e (at $A=3$)
A ($BaTiO_3$, Ba/Ti=1.003)	1350 °C, 30 h, air	1300 °C, 30 h, $P_{O_2} \sim 10^{-17}$ atm	5.96[b]	36.8 (26.5, 30.5)	Eq. (2) [Eq. (4)]	7.6
B ($BaTiO_3$, Ba/Ti=1.003)	1300 °C, 30 h, $P_{O_2} \sim 10^{-17}$ atm		5.96[b]	36.8 (18.2, 46.5)	Eq. (2) [Eq. (4)]	8.5
C ($BaTiO_3$, Ba/Ti=1.003)	1350 °C, 30 h, air	1000 °C, 100 h, $P_{O_2} \sim 10^{-18}$ atm	5.96[b]	1.97 (1.89, 5.12)	Eq. (2) [Eq. (4)]	12.65
D ($SrTiO_3$, Sr/Ti ~ 1)	1300 °C, 30 h, $P_{O_2} \sim 10^{-17}$ atm		6.1[c]	28.7 (10.5, 28.5)	Eq. (2) [Eq. (4)]	9.8 (HT) 4.3 (LT)
5[a] ($BaTiO_3$ single crystal)		1000 °C, 10 h, 40 ccm H_2/N_2		1.90[a]	Hall effect at 400 K	11.5[a]
6[a] ($BaTiO_3$ single crystal)		1050 °C, 10 h, 40 ccm H_2		6.10[a]	Hall effect at 400 K	10.5[a]
8[a] ($BaTiO_3$ single crystal)		1250 °C, 20 h, 90 ccm H_2		34.6[a]	Hall effect at 400 K	6.57[a]

[a]Reference 16.
[b]Reference 18.
[c]Reference 19.

als where reduction processes can enhance the n-type carrier concentrations and, in turn, affect the thermopower and conductivity of the materials. A second goal of this work is to probe the relative differences in the Seebeck effect and conductivity near room temperature in highly reduced $BaTiO_3$ and $SrTiO_3$ materials, noting the impact of the structural transitions and nonstoichiometry distributions.

II. EXPERIMENT

Polycrystalline $BaTiO_3$ and $SrTiO_3$ were fabricated using a modified citrate process[15] and conventional solid-state powder processing techniques, respectively. X-ray powder diffraction confirms that all samples are single phase. To obtain reduced samples, we have used two different pathways. In the first approach, samples were sintered in air and a post-annealing reduction step was conducted. Undoped $BaTiO_3$ was first sintered in air at 1350 °C for 30 h, resulting in samples having greater than 94% theoretical density. The samples were subsequently reduced by annealing at 1300 or 1000 °C for 30–100 h in oxygen partial pressures (P_{O_2}) of $\sim 10^{-17}$ and $\sim 10^{-18}$ atm, respectively. The reducing atmospheres were produced using gas mixtures of N_2-H_2, and the oxygen partial pressure was measured with a Y-stabilized zirconia oxygen sensor (DS Probe, Australian Oxytrol Systems Pty. Ltd.). Upon completion of the annealing step, samples were quenched at room temperature. As an alternative to reducing air fired ceramics, $BaTiO_3$ and $SrTiO_3$ were sintered at 1300 °C for 30 h under $P_{O_2} \approx 10^{-17}$ atm. The synthesis conditions and estimated free-electron concentrations are summarized in Table I. The electron concentrations were estimated using annealing conditions (T and P_{O_2}) and enthalpies for the reduction reaction, as will be discussed below. Seebeck coefficients were measured in a MMR Technologies SB-100 Programmable Seebeck Controller. An Ohmic contact was made to the samples by sputtering a 10 nm layer of Ti overcoated with 100 nm of Pt. Electrical contact to the probes was made using silver epoxy (Epo-tek H20E). Ohmic contact was confirmed by impedance measurements using a Solartron SI 1287 electrochemical interface with model 1255B frequency response analyzer. The dc electrical conductivity versus temperature was measured with a HP 3478A multimeter from 150–525 K using a four-point technique. Transition temperatures in the $BaTiO_3$ materials were characterized using a differential scanning calorimeter (DSC) (DSC2920, TA Instruments). The DSC measurements were carried out under dry nitrogen during heating at 180 °C, holding the sample isothermally at 180 °C for 5 min and then cooling from 180 to −10 °C at a rate of 5 °C/min.

The transmission electron microscopy studies were made by cutting samples out of the ceramics and then grinding the piece to about 30 μm thickness. These samples were mounted to transmission electron microscopy (TEM) 3 mm copper grids and adhered with epoxy. These samples were then ion beam thinned using an EA Fishione Model 3000 ion mill operating at 4–5 kV to accelerate an ionized Argon beam (5 mA current) with an incidence angle of 10–12°. The samples were mounted in a liquid-nitrogen-cooled stage during the thinning process to minimize interdiffusion and migration of oxygen vacancies. Samples were then thinned to electron transparency. Microstructure and microchemical studies were performed using a JEOL transmission electron microscope equipped with a field emission gun (JEOL 2010F) operating at 200 kV. Electron energy loss spectroscopy (EELS) was performed with a Gatan Enfina parallel electron energy loss (EEL) spectrometer attached to the

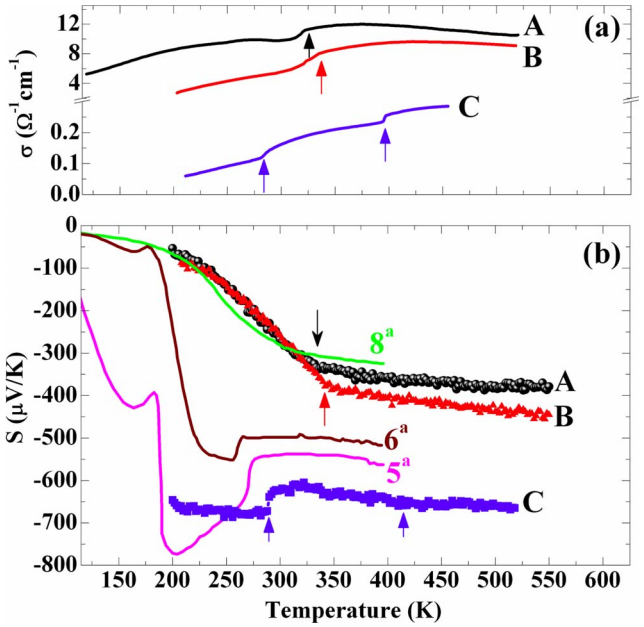

FIG. 1. (Color online) (a) Seebeck coefficients and (b) electrical conductivity as a function of temperature for pure $BaTiO_3$ (Ba/Ti =1.003) sintered at 1350 °C in air and then quenched from 1300 °C at $P_{O_2} \sim 10^{-17}$ atm (sample A) and 1000 °C at $P_{O_2} \sim 10^{-18}$ atm (sample C). Sample B was sintered at 1300 °C at $P_{O_2} \sim 10^{-17}$ atm for 30 h. 5^a, 6^a, and 8^a represent samples 5, 6, and 8 in Fig. 3(a) from Ref. 16.

JEOL 2010F microscope. The energy resolution at the zero-loss peak is approximately 1.1 eV full width at half maximum. EELSs were recorded in TEM-diffraction mode with a collection angle of 14 mrad and were analyzed using GATAN DIGITAL MICROGRAPH software.

III. RESULTS AND DISCUSSION

Both electrical conductivity and thermopower depend on the charge carrier concentration and mobility. In general, these properties together enhance the figure of merit. However, in reduced perovskite materials, the correlation is much more complicated with temperature owing to phase transitions and the conduction mechanisms shown.

Figure 1 shows the electrical conductivities and Seebeck coefficients as a function of temperature for pure $BaTiO_3$ sintered and annealed under different low P_{O_2} conditions to enhance the electrical conductivity through the compensation of oxygen vacancies, $n_e \approx 2[V_O^{\bullet\bullet}]$. n_e and the concentration of oxygen vacancies both increase via the reduction reaction,

$$O_O^X \Leftrightarrow \frac{1}{2}O_2 + V_O^{\bullet\bullet} + 2e'. \quad (1)$$

It was found that the conductivity and thermopower both exhibited anomalies at temperatures associated with structural phase transitions. As shown in Fig. 1(a), the electrical conductivities of samples A and B both have metallic behavior above 320 K. Below 320 K, there is a broad continuous transition to a semiconducting state that is associated with a

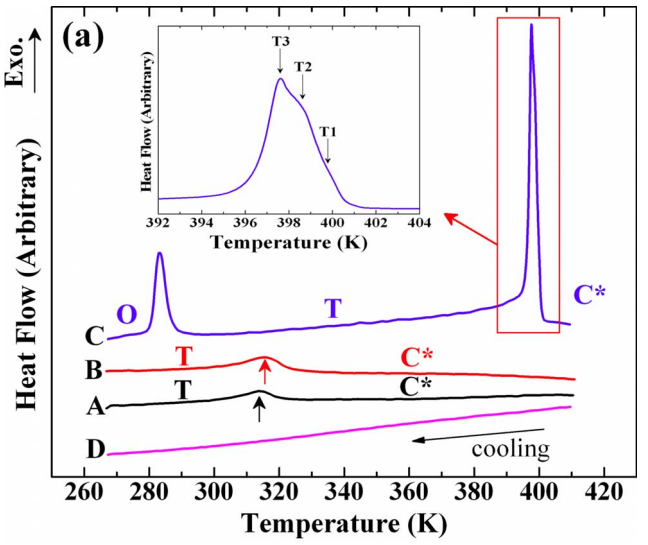

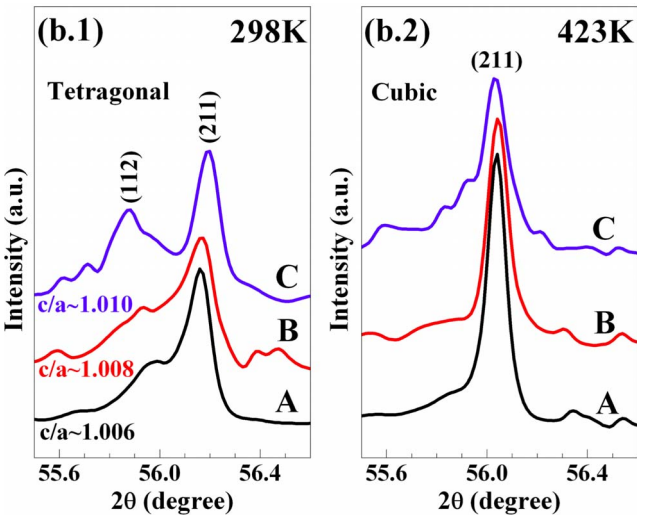

FIG. 2. (Color online) (a) DSC curves and XRD patterns at (b.1) 298 K and (b.2) 423 K for samples A, B, C, and D. C^* stands for cubic; T for tetragonal; O for orthorhombic phase. The scan rate of DSC was 5 °C/min. $T1$, $T2$, and $T3$ present different phase transition temperatures.

structural phase transition from the $Pm3m$ to the $P4mm$ phase (see Fig. 2). The nature of the first-order phase transitions is confirmed by the presence of latent heat anomalies observed in the DSC measurements. Peak splitting in the x-ray diffraction (XRD) patterns at different temperatures indicates the crystal structure (see Fig. 2). The c/a ratio decreases with increasing reduction level; this is self-consistent with the depressed latent heat peak as oxygen vacancies would be expected to shift the phase transition temperature (T_{CT}) to lower temperatures.[17] The conductivity data for sample C, on the other hand, demonstrate semiconducting behavior over the whole temperature range measured, with steplike changes at each of the first-order phase transitions present in the lightly reduced sample ($Pm3m$ to $P4mm$ near 400 K and $P4mm$ to $Cmm2$ near 285 K). The discontinuous conductivity decrease in sample C can be understood as a result of the decrease in crystal symmetry associated with each transition.

The corresponding thermopower data, as seen in Fig. 1(b), show two different trends for the reduced $BaTiO_3$ samples; the figure also demonstrates that the thermopower coefficients are strongly correlated with the reduction level. Samples A and B (which are heavily reduced) show a monotonic increase in thermopower between 200 and 320 K. Above that temperature the rate of increase drops. In contrast, the less reduced $BaTiO_3$ materials (e.g., sample C) which are semiconducting in the measured temperature range, demonstrate a higher thermopower magnitude. From 200 to 285 K the thermopower is almost invariant to temperature, and between 300 to 550 K there is a slight increase in magnitude. These trends have recently been noted in a $BaTiO_3$ single-crystal study by Kolodiazhnyi.[16] Data from this reference are also included for comparison.

In comparing the structural data from Fig. 2 to the thermopower data, it is evident that the ferroelectric (*P*4*mm*)-ferroelectric (*Cmm*2) phase transition around 285 K influences the thermopower in sample C and data 5^a and 6^a from Ref. 16. It is also likely that the anomaly around 180 K, which is clearly evident in samples 5^a and 6^a, is a result of the *Cmm*2-*R*3*m* transition. It is interesting that the *Pm*3*m*-*P*4*mm* transition does not significantly influence the thermopower in sample C, even though there are anomalies for this transition in the conductivity data. In the more reduced samples (A, B, and 8^a), we observed influence of the ferroelectric transition (*Pm*3*m*-*P*4*mm*), which is suppressed to lower temperatures. Here the transitions are closely related to a change in the slope in the temperature dependence of the thermopower.

From the conductivity data in Fig. 1(a), we noted that for samples A and B we have a metal-insulator transition. Applying the Mott criterion as an approximation, we would expect there exists a critical electronic concentration. The bulk concentration of oxygen vacancies and the associated carrier concentration can be estimated using a traditional bulk defect chemistry approach. It is noted, though, that this approach is based on dilute and homogeneous boundary conditions and maybe be of limited accuracy for these high concentrations of defects.

The total concentration at equilibrium between the system and the surrounding atmosphere is based on the reaction given in Eq. (1). In addition, the Bröuwer approximation can be made for full electronic compensation of the oxygen vacancies such that $n_e \approx 2[V_O^{\bullet\bullet}]$. Using this approximation and the enthalpy for doubly ionized oxygen vacancy (Δh_{Re}), 5.96 ± 0.15 eV for $BaTiO_3$ (Ba/Ti=1.003), which was determined through electrical conductivity measurements at various oxygen partial pressures (P_{O_2}) and temperatures,[18] we obtain

$$n_e = M 2^{1/3} K_0^{1/3} P_{O_2}^{-1/6} \exp\left(\frac{-\Delta h_{Re}}{3 k_B T}\right), \tag{2}$$

where M is the number of oxygen sites per unit volume (cm^{-3}); K_0 is a constant including an entropy term; k_B is Boltzmann's constant; T is the absolute temperature of the annealing condition (Kelvin). Assuming an equilibrium or a quasiequilibrium state for these samples, the n_e approximated for samples A and B is $\sim 3.68 \times 10^{20}/cm^3$ and $\sim 1.97 \times 10^{19}/cm^3$ for sample C (see Table I). The carrier concentrations for metallic behavior are also in good agreement with the critical carrier concentration based on the Mott criterion, $1.6 \times 10^{20}/cm^3$ in $BaTiO_{3-\delta}$.

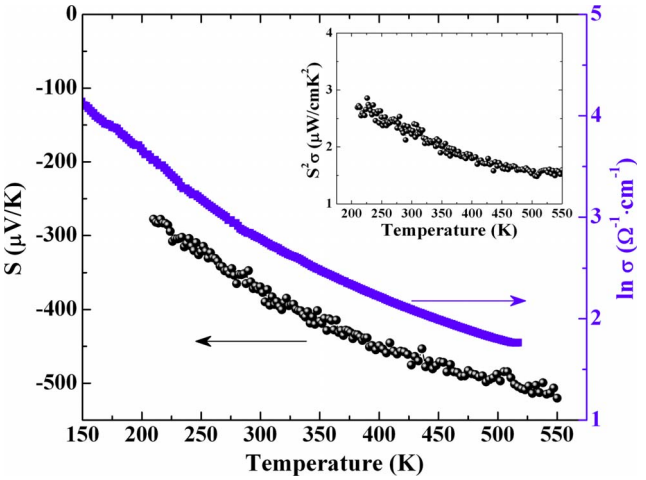

FIG. 3. (Color online) Thermopower (S), electrical conductivity (σ), and power factor ($S^2\sigma$) as a function of temperature for reduced $SrTiO_{3-\delta}$ (sample D).

To contrast with reduced $BaTiO_3$, reduced $SrTiO_3$ ceramics were measured over the same temperature range. The thermopower, electrical conductivity, and power factor ($S^2\sigma$) are all shown in Fig. 3. The conductivity for the heavily reduced $SrTiO_{3-\delta}$ shows metallicklike temperature dependence. The increase in thermopower with temperature is also consistent with the metallic conductivity. There are no marked anomalies for $SrTiO_{3-\delta}$, which is reasonable as we do not expect any displacive phase transitions in this temperature range [see Fig. 2(a), sample D]. These differences also support the evidence of a ferroelectric-thermoelectric effect in the $BaTiO_3$ material.

Using the enthalpy for reduction, $\Delta h_f = 6.1$ eV,[19] for $SrTiO_3$ at the annealing temperature, we estimate the carrier concentration to be $2.87 \times 10^{20}/cm^3$, which is higher than the concentration required by the Mott criterion in $SrTiO_{3-\delta}$, $\sim 1 \times 10^{18}/cm^3$.[13] So from the reduction conditions used, it is anticipated that a metallic conduction process should be dominant, as observed in Fig. 3.

The local reduction was investigated in more detail with EELS and high-resolution electron microscopy. As shown in Fig. 4, distributed defect regions with differing degrees of reduction are observed. The different regions are shown on the micrographs labeled A1 and A2 and have oxygen vacancy concentrations of $\sim 2.7 \times 10^{21}/cm^3$ ($SrTiO_{2.8\pm0.04}$) and $\sim 6 \times 10^{21}/cm^3$ ($SrTiO_{2.62\pm0.05}$), respectively. The regions containing high oxygen vacancy concentrations should give rise to a reduction from Ti^{4+} to Ti^3, which is consistent with the observed lack of splitting of the Ti $L_{2,3}$ peak in the EELS spectra [see Fig. 4(b)]. The EELS technique for determining these nonstoichiometries, along with the calibration and experimental details, is presented elsewhere.[20] It is anticipated that these three-dimensional (3D) "wormhole"-like defects give rise to the strong metallic behavior and, with the matrix,

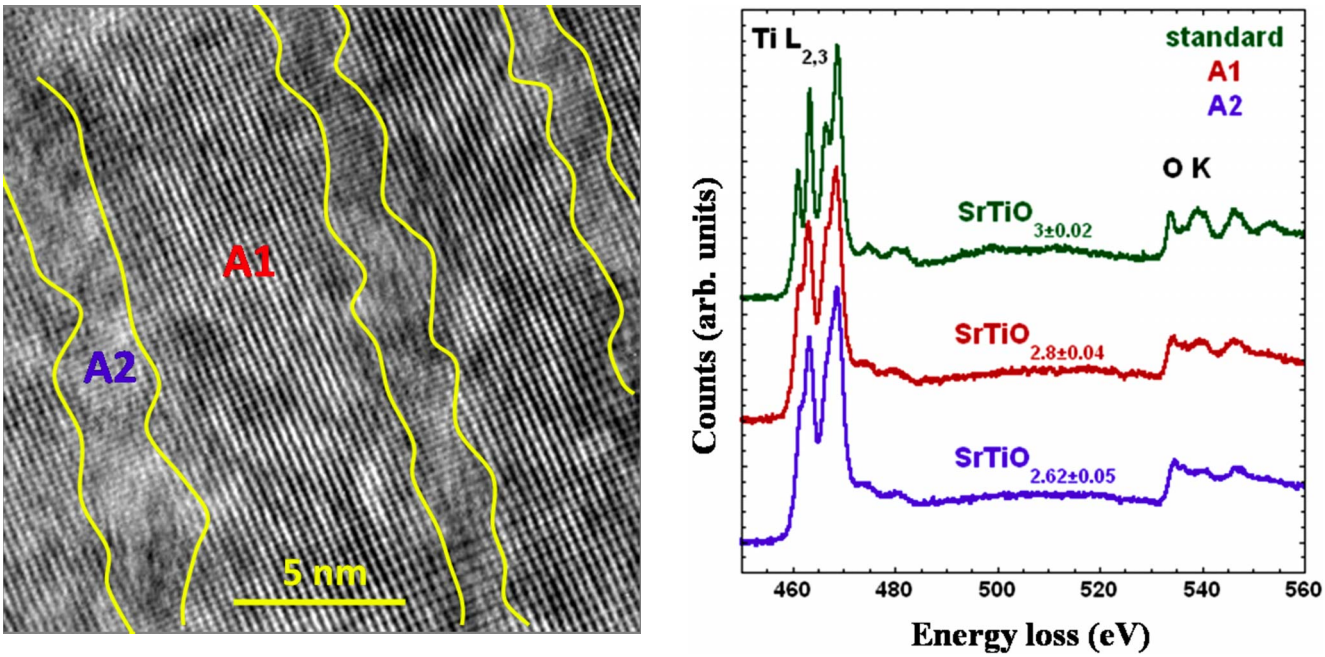

FIG. 4. (Color online) (a) TEM image and (b) EELS data for $SrTiO_3$ sintered at 1300 °C for 30 h under $P_{O_2} \sim 10^{-17}$ atm (sample D). A1: more lightly reduced areas; A2: more highly reduced areas.

provide complex conduction and thermopower mechanisms. Some regions have conduction controlled by hopping processes or band conductions, while others have a free (or nearly free) electron-controlled conduction processes. It is also well known that random vacancies, local lattice distortions, structures containing void spaces, etc. can be the sites for phonon scattering,[3] which in turn leads to the decrease in thermal conductivity. This provides a possible means of increasing the figure of merit, *ZT*. Recently, Yu *et al.*[21] reported that a high oxygen vacancy concentration reduced the thermal conductivity in $Sr_{1-x}La_xTiO_{3-\delta}$ by a factor of 4.3. It is anticipated that the wormhole defects, and the associated strain in the perovskite crystal structure, can suppress the thermal conductivity due to the phonon scattering and can cause strong electron-lattice interactions which enhance the thermopower.

The local heterogeneity will certainly indicate that irrespective of sintering in low P_{O_2} and/or annealing in reduced atmosphere there is local compositional heterogeneity in the highly nonstoichiometric materials. We anticipate that the percolation and the volume fraction of the regions with different oxygen and carrier concentrations will dominate the macroscopic properties. Despite this microstructural complexity and potential complications associated with the structural phase transitions, the temperature and reduction dependences of the thermopower on these perovskite oxide materials are considered with conventional models. We report here the relevance of these models in different temperature regions and carrier concentrations.

At higher temperatures (above the phase transition temperatures in the paraelectric phase), the thermopower in all samples is less sensitive to temperature. As explained above, samples A, B, and D all are heavily reduced and show metallic behavior. Within a degenerate semiconductor model, metal-like behavior, assuming a temperature-independent mean-free path, the thermopower has a temperature dependence that is typically described in terms of a degenerate Fermi gas model,[22,23]

$$S = C_n m^* n_e^{-2/3} T, \tag{3}$$

where the constant C_n contains only fundamental physical constants, $C_n = (8\pi^{8/3}k_B^2)/(3^{5/3}h^2 e)$; m^* is the electron effective mass; n_e is the carrier concentration; and h is Planck's constant. Although the conductivity for all of the heavily reduced oxides shows metallic behavior at high temperatures, the degenerate Fermi gas model can only be applied for $SrTiO_{3-\delta}$ sample D at low temperatures as shown in Fig. 5. Above 350 K, the thermopower follows the nondegenerate semiconductor model. For nondegenerate semiconductors, the Seebeck coefficients (S) can be described by[13]

$$S = -k_B/e[\ln(N_C/n_e) + A], \tag{4}$$

where the electron transport or scattering factor is A, which depends on the scattering mechanism and usually ranges between 0 and 4, and the effective density of states in the conduction band, N_c, has the usual temperature dependence: $N_C(T) = 2\cdot[(2\pi m^* kT)/h^2]^{3/2}$. A plot of S vs $\log T$ should yield a slope of $-298\ \mu V/K/T$ decade.[22] The data for $BaTiO_{3-\delta}$ samples A and B above 350 K yield slopes of -272 ± 15 and $-307 \pm 10\ \mu V/K/$decade, respectively [see Fig. 5 (inset)]. Therefore, the thermopower follows a nondegenerate semiconductor model even when the conductivity-temperature curve shows metallic behavior. The heavily reduced $SrTiO_{3-\delta}$ (sample D) also shows good fitting to the nondegenerate semiconductor model at higher temperatures; below 300 K the Seebeck coefficient is proportional to T as is consistent with metallic behavior,[24] so there is a crossover in the thermopower dependence. It is believed that the non-

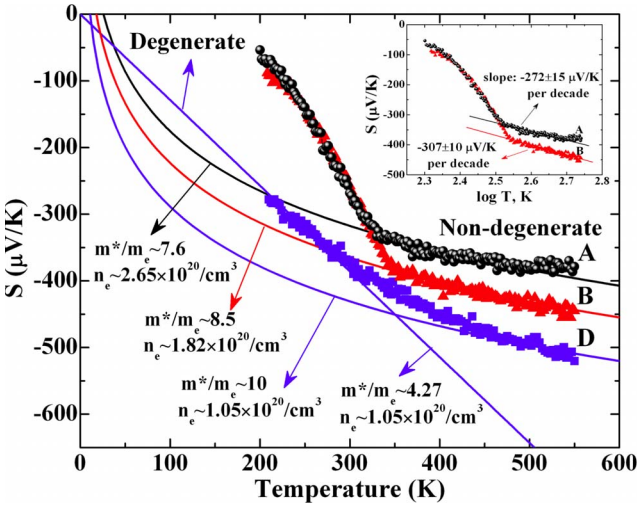

FIG. 5. (Color online) Seebeck coefficients as a function of temperature for samples A, B, and D. The solid lines for each sample represent the theoretical Seebeck coefficients calculated using a nondegenerate semiconducting model for samples A, B, and D or a degenerate Fermi gas model for sample D. The inset shows the relationship between S and log T.

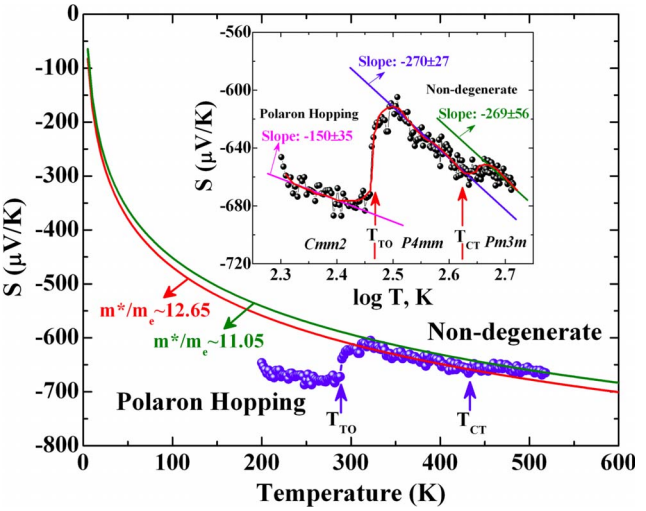

FIG. 6. (Color online) Seebeck coefficients as a function of temperature for sample C. The solid lines represent the theoretical Seebeck coefficients calculated using a nondegenerate semiconductor model. The inset shows the slopes from S vs log T for each region. T_{CT} is the $Pm3m$-$P4mm$ transition temperature and T_{TO} is the $P4mm$-$Cmm2$ transition temperature.

degenerate semiconductor behavior of the thermopower even in a regime showing metallic behavior for the conductivity results from the heterogeneous nonstoichiometry; the thermopower is dominated by the less reduced regions, and the metallic conductivity is controlled by the highly reduced regions in microstructures similar to those shown in Fig. 4.

It is interesting to extract the effective electron mass and carrier concentrations for the degenerate and nondegenerate models of the thermopower data. Fitting Eq. (4) with different scattering factors, $A=3$ and $A=4$ assuming high scattering factors with the heterogeneous defects, we note that the effective mass and electron concentrations are in a reasonable range, as summarized in Table I.

For sample C, which has a smaller carrier concentration, the high-temperature data (Fig. 6) show the expected temperature dependence for a nondegenerate semiconductor. The semiconducting nature is demonstrated by the temperature dependence of the electrical conductivity $(d\sigma/dT>0)$ as shown in Fig. 1(a). It is noted that around 420 K there is a small step, which coincides with the $Pm3m$-$P4mm$ phase transition temperature. The data are well described by the nondegenerate semiconductor model on either side of the transition. Fitting the data for $Pm3m$ and $P4mm$ phase regions independently yields slopes of -269 ± 56 and -270 ± 27 μV/K/decade, respectively [see Fig. 6 (inset)]. However, at temperatures below T_{TO} ($P4mm$-$Cmm2$ transition temperature), the slope is -150 ± 35 μV/K/decade, and this departs from the nondegenerate semiconductor model. The fact that at lower temperatures the data do not exhibit the temperature dependence for a nondegenerate semiconductor in spite of the conductivity of $d\sigma/dT>0$ in Fig. 1(a) implies that the semiconductor behavior arises from an alternative conduction mechanism, such as a hopping process, for the $Cmm2$ phase. If this is the case, the thermopower can be approximated by the Heikes formula.[25] As pointed out by Chaikin and Beni,[26] there are modifications to this formula that can better address the spin interactions of the electrons; we therefore use

$$S=-k_B/e\ \ln[(2-c)/c], \tag{5}$$

where $c=[Ti^{3+}]/[Ti^{4+}]$. As shown in Figs. 7(a) and 7(b), the TEM and EELS data for $Ba_{1-x}Ca_{x+y}Ti_{1-y}O_{3-y-\delta}$ $(x+y=0.05,\ x\gg y)$, which has the same thermal history as sample C, show a local reduction in Ti^{4+} to Ti^{3+}. Again, this is inferred from the lack of the characteristic splitting of the Ti $L_{2,3}$ peak in the EELS spectra. If we take $[Ti^{3+}]=n_e$ $(\sim1.97\times10^{19}/cm^3)$ and assume $[Ti^{3+}]+[Ti^{4+}]$ is equal to the concentration of Ti sites per unit volume $(\sim1.527\times10^{22}/cm^3)$, then an estimate of -633 μV/K for the Seebeck coefficient is obtained. This is in good agreement with the experimentally measured value of ~-670 μV/K. However, it is again anticipated that the heterogeneity of defects and structures may impact the true behavior of the thermopower.

The heterogeneity is also observed in the DSC data [see Fig. 2 (inner figure)] showing multiple latent heat peaks, consistent with the locally different phase transitions that are sensitive to the nonstoichiometry of the oxide.[27] The ferroelectric phase and the heterogeneity of the microstructure through the reduction process affect the nature of the mechanism controlling the thermopower in the $BaTiO_3$ system. The nondegenerate models appear reasonable for the semiconducting $BaTiO_3$ (sample C) in the $Pm3m$ and $P4mm$ phases. However, below the $P4mm$-$Cmm2$ phase transition there is a strong departure from this behavior, and a hopping process seems more applicable. This is further confirmed through considering the temperature dependence of the conductivity. Within the variable-range hopping model,[12,28] the conductivity is given by $\sigma=A\exp[-(T_0/T)^{1/4}]$, where A and T_0 are

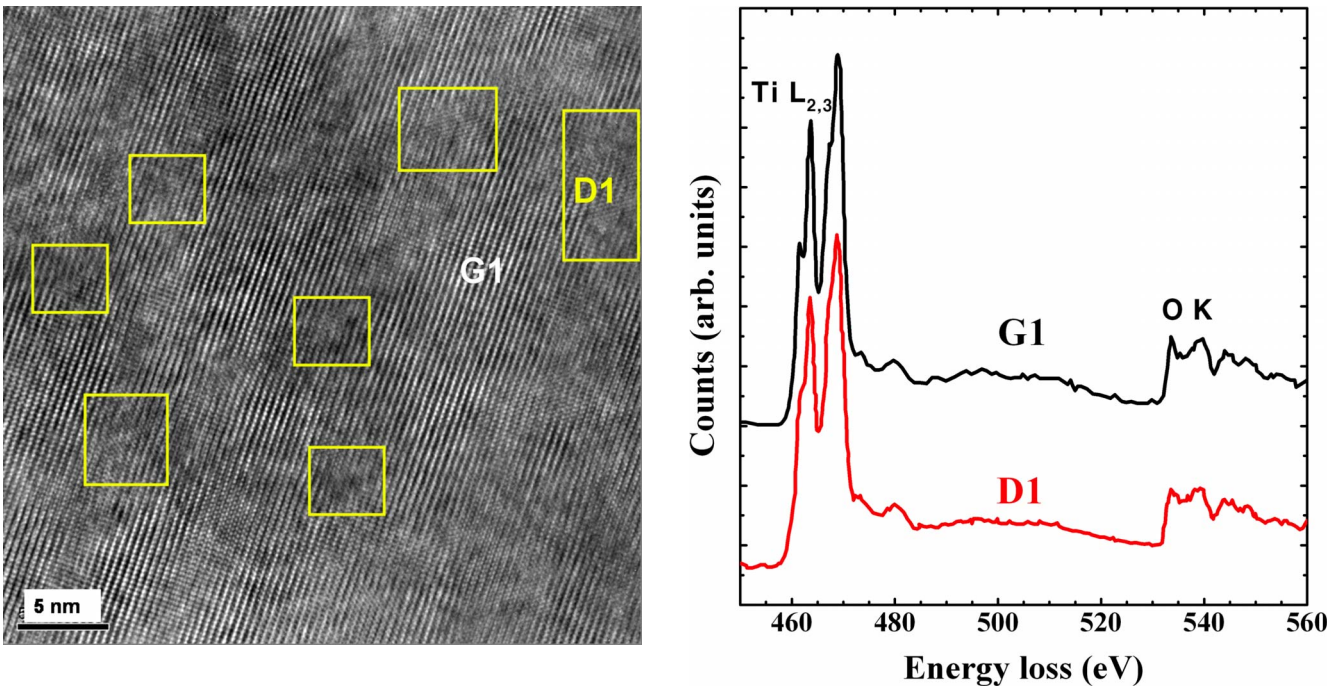

FIG. 7. (Color online) (a) TEM image and (b) EELS data for $Ba_{1-x}Ca_{x+y}Ti_{1-y}O_{3-y-\delta}$ $(x+y=0.05,\ x \gg y)$ sintered at 1350 °C in air for 30 h and then quenched from 1000 °C under $P_{O_2} \sim 10^{-18}$ atm. D1: defective, more heavily reduced area; G1: nondefective area.

constants. At low temperatures a plot of ln σ versus $T^{-1/4}$ yields a linear fit, clearly demonstrating variable-range hopping in the *Cmm*2 phase (see Fig. 8).

As sample C approaches 200 K upon cooling, there is a decrease in thermopower. From the data of Kolodiazhnyi,[16] there is much more clear evidence of this effect. It appears that this anomaly results from the *Cmm*2-*R*3*m* ferroelectric–ferroelectric transition. So ultimately there is additional physics to be investigated in this regime. Such anomalous decreases in thermopower are unusual, but work by Töpfer and Goodenough[29] may be relevant to account for such behavior. These authors observed similar behavior in a $LaMnO_3$ perovskite, which has an octahedral tilt transition between the ferroelastic (*Pbnm*)-ferroelastic ($R\bar{3}c$) phases at T_{OR}. It was suggested that the mobile polaronic carriers in a narrow band are increasingly trapped upon approaching the tilt phase transition temperature (T_{OR}), which results in an increase in thermopower. Below T_{OR} a broadening of the width of the narrow band releases the trapped carriers, and the net result is a decrease in the magnitude of the thermopower. It has also been suggested that the lower conductivity below T_{OR} results from the condensation of conduction electrons into a "vibronic" state associated with a strong coupling of the mobile carriers to cooperative oxygen displacements along the Mn-O bond axes.[29,30] This would suggest that a theoretical model taking account of ferroelectric phase transitions and nonstoichiometric heterogeneity should be further investigated to describe the reduced perovskite titanates.

IV. CONCLUSIONS

The *n*-type thermopower in perovskite oxides was enhanced by reduction reactions, which also control the carrier concentrations for electrical conductivity. The thermopower and conductivity showed anomalies associated with the ferroelectric phase transitions in $BaTiO_3$. The behavior of the thermopower anomalies depends on the ionic and electronic defect concentrations generated by the reduction reaction. Microstructural and EELS analysis reveals that either sintering or annealing in a reducing atmosphere leads to heterogeneous nonstoichiometries; the highly reduced meandering regions are termed wormholes. In highly reduced $SrTiO_{3-\delta}$, there is the expected metallic behavior in the conductivity; at low temperatures there is degenerate Fermi gas thermopower behavior, but above 450 K the thermopower is dominated by

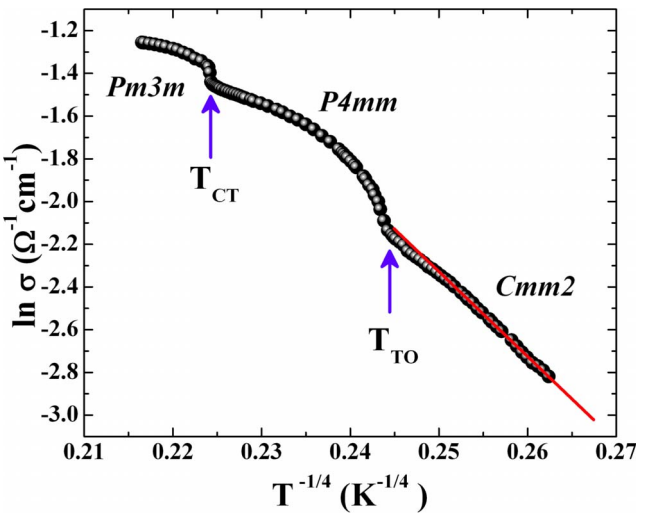

FIG. 8. (Color online) Electrical conductivity (ln σ) vs $T^{-1/4}$ for sample C. T_{CT} is the *Pm*3*m*-*P*4*mm* transition temperature and T_{TO} is the *P*4*mm*-*Cmm*2 transition temperature.

a nondegenerate semiconductor mechanism. This suggests that in highly reduced oxides with heterogeneous nonstoichiometry, there can be decoupling between the thermopower and electrical conductivity at high temperatures; the less reduced regions control the macroscopic thermopower response, while the conductivity is controlled by the metallic, highly reduced regions.

Heavily reduced $BaTiO_{3-\delta}$ is metallic in terms of the macroscopic conductivity, and the *Pm*3*m*-*P*4*mm* phase transition produces an anomaly in both the conductivity and thermopower measurements. The thermopower is described by nondegenerate semiconductor behavior in the paraelectric phase, while the ferroelectric phase requires a more complex mechanism, such as the carrier trap-release processes and the vibronic state, as described Töpfer and Goodenough.[29]

In the less reduced semiconducting $BaTiO_{3-\delta}$, both the *Pm*3*m* and *P*4*mm* phases have thermopowers described by nondegenerate semiconductor models and show a small anomaly at the transition temperature. In the *Cmm*2 phase, the conductivity changes to localized variable hopping and the thermopower follows the modified Heikes formula for spin interactions. Near and below the *Cmm*2-*R*3*m* transition, there is an anomalous decrease in the thermopower; this again may be related to the carrier trap-release mechanism. It was found that the conductivity and thermopower temperature dependence are strongly related to observed heterogeneous nonstoichiometries and phase transitions. Models are required to fully understand the ferroelectric-thermoelectric effects. From a technological perspective, the relatively high coefficients coupled with the microstructural interactions offer opportunities to engineer enhanced power factors in reduced perovskite ferroelectric oxides for more efficient thermoelectric devices.

ACKNOWLEDGMENTS

This study is based on work supported by the National Science Foundation as part of the Center for Dielectric Studies under Grant No. 0628817 and partial support by MRI (Materials Research Institute) for R.H.T.W.

*leesoonil@gmail.com

[1] T. J. Seebeck, Abhandlungen der Königlich Preussischen Akademie der Wissenschaften, Berlin, 1821, p. 289.
[2] H. J. Goldsmid, *Thermoelectric Refrigeration* (Plenum, New York, 1964).
[3] G. J. Snyder and E. S. Toberer, Nature Mater. **7**, 105 (2008).
[4] G. Slack, in *CRC Handbook of Thermoelectrics*, edited by D. M. Rowe (CRC, Boca Raton, 1995).
[5] G. Chen, M. S. Dresselhaus, G. Dresselhaus, J.-P. Fleurial, and T. Caillat, Int. Mater. Rev. **48**, 45 (2003).
[6] H. Ohta, Mater. Today **10**, 44 (2007).
[7] I. Terasaki, Y. Sasago, and K. Uchinokura, Phys. Rev. B **56**, R12685 (1997).
[8] T. Okuda, K. Nakanishi, S. Miyasaka, and Y. Tokura, Phys. Rev. B **63**, 113104 (2001).
[9] C. Yu, M. L. Scullin, M. Huijben, R. Ramesh, and A. Majumdar, Appl. Phys. Lett. **92**, 092118 (2008).
[10] L. D. Hicks and M. S. Dresselhaus, Phys. Rev. B **47**, 12727 (1993).
[11] H. P. R. Frederikse, W. R. Thurber, and W. R. Hosler, Phys. Rev. **134**, A442 (1964).
[12] T. Kolodiazhnyi, A. Petric, M. Niewczas, C. Bridges, A. Safa-Sefat, and J. E. Greedan, Phys. Rev. B **68**, 085205 (2003).
[13] P. A. Cox, *Transition Metal Oxides* (Oxford University Press, New York, 1992), p. 158.
[14] H. Ihrig and D. Hennings, Phys. Rev. B **17**, 4593 (1978); P. Bernasconi, I. Biaggio, M. Zgonik, and P. Günter, Phys. Rev. Lett. **78**, 106 (1997); P. W. Anderson, Phys. Rev. **109**, 1492 (1958).
[15] S. Lee, Z. K. Liu, and C. A. Randall, J. Am. Ceram. Soc. **92**, 222 (2009).
[16] T. Kolodiazhnyi, Phys. Rev. B **78**, 045107 (2008).
[17] K. H. Härdtl and R. Wernicke, Solid State Commun. **10**, 153 (1972).
[18] S. Lee, R. D. Levi, and C. A. Randall (unpublished).
[19] R. Moos and K. H. Härdtl, J. Am. Ceram. Soc. **80**, 2549 (1997).
[20] G. Y. Yang, S. I. Lee, Z. J. Liu, C. J. Anthony, E. C. Dickey, Z. K. Liu, and C. A. Randall, Acta Mater. **54**, 3513 (2006).
[21] C. Yu, M. L. Scullin, M. Huijben, R. Ramesh, and A. Majumdar, Appl. Phys. Lett. **92**, 191911 (2008).
[22] N. W. Ashcroft and N. D. Mermin, *Solid State Physics* (Harcourt, Inc., Orlando, 1976); J. B. Goodenough, Prog. Solid State Chem. **5**, 145 (1971).
[23] R. Moos, A. Gnudi, and K. H. Hardtl, J. Appl. Phys. **78**, 5042 (1995).
[24] Y. Klein, S. Hébert, A. Maignan, S. Kolesnik, T. Maxwell, and B. Dabrowski, Phys. Rev. B **73**, 052412 (2006).
[25] R. R. Heikes and R. W. Ure, Jr., *Themoelectricity: Science and Engineering* (Interscience, New York, 1961), p. 77.
[26] P. M. Chaikin and G. Beni, Phys. Rev. B **13**, 647 (1976).
[27] S. Lee, Z. K. Liu, M. H. Kim, and C. A. Randall, J. Appl. Phys. **101**, 054119 (2007).
[28] N. F. Mott, *Metal-Insulator Transitions* (Taylor and Francis, London, 1974).
[29] J. Töpfer and J. B. Goodenough, Chem. Mater. **9**, 1467 (1997).
[30] J.-S. Zhou, W. Archibald, and J. B. Goodenough, Nature (London) **381**, 770 (1996).